Defect-mediated nucleation of α-iron in Au-Fe alloys

P. Fratzl, F. Langmayr, and Y. Yoshida*
Institut für Festkörperphysik der Universität Wien, Strudlhofgasse 4, A-1090 Wien, Austria
(Received 28 January 1991)

The low-temperature magnetic properties of Au-Fe alloys, such as spin-glass or mictomagnetic behavior, are known to be dependent on thermal history and therefore on the atomic order in the sample. The nature of this order is still controversial, and the discussion includes the presence of short-range order as well as the precipitation of Guinier-Preston (GP) zones. It is frequently neglected in this context that there is a miscibility gap in Au-Fe at low temperatures, where ferromagnetic α-iron should coexist with the solid solution. The conditions for α-iron nucleation have not been studied systematically in the range of compositions, where spin-glass or mictomagnetic behavior appears. We have used a combination of Mössbauer spectroscopy, x-ray diffraction, and small-angle scattering to investigate the nucleation of α-iron in $Au_{0.85}Fe_{0.15}$ and $Au_{0.75}Fe_{0.25}$: (1) This nucleation appeared to be a discontinuous process related to the presence of a high dislocation density. (2) No homogeneous precipitation, like the formation of GP zones, was observed. (3) All experimental results seem to be in agreement with the hypothesis of a $(1\frac{1}{2}0)$ special-point short-range ordering in the solid solution.

I. INTRODUCTION

The alloy system Au-Fe has been extensively investigated for its interesting low-temperature magnetic properties known as spin-glass or mictomagnetic behavior.[1] Very soon it was recognized that these magnetic properties are dependent not only on the sample composition, but also on their thermal treatment,[2] which suggests that the magnetism is strongly influenced by the atomic short-range order (ASRO).[3,4] Nevertheless, there were only a few attempts to elucidate the ASRO in this system. Measurements of diffuse x-ray scattering by Dartyge, Bouchiat, and Monod[5] of $Au_{0.81}Fe_{0.19}$ showed a diffuse maximum at the $(1\frac{1}{2}0)$ reciprocal lattice point and streaks in $\langle 210 \rangle$ directions. This was interpreted in terms of an ASRO consisting of Fe-rich plates oriented along (420) lattice planes, a result confirmed later with the use of neutron scattering[6] and synchrotron radiation.[7,8] On the other hand, Mössbauer spectroscopy measurements of quenched samples[9] as well as recent high-temperature Mössbauer experiments for $Au_{1-x}Fe_x$ with $1 < x < 15$ at. %,[10] revealed a negative first ASRO parameter. This led to the conclusion that the ASRO might be a $(1\frac{1}{2}0)$ special-point ordering,[11] consisting of a succession of iron-rich and iron-poor (420) planes. Alternatively, based mainly on investigations by electron microscopy[8,12,13] and small-angle scattering,[8] the formation of Fe precipitates similar to GP zones was proposed for $Au_{1-x}Fe_x$ with $11 < x < 35$ at. %.

A fact that is frequently overlooked in this context is the existence of a miscibility gap at higher Fe concentrations, where the thermodynamic equilibrium corresponds to a mixture of α-iron and Au-Fe solid solution.[14,15] This is the more important for the discussion of the ASRO, as some of the investigations were carried out with samples treated thermally at temperatures within the miscibility gap,[8,13] while others concern the stable solid solution.[9,10] It would indeed be extremely surprising to find similar states of atomic order in both cases. For $Au_{1-x}Fe_x$ with higher Fe concentrations ($x > 0.3$), the nucleation of α iron is well known[16–18] to occur discontinuously at lattice defects like dislocations or grain boundaries, giving rise to lamellar or Widmanstätten-type microstructures,[18] i.e., interconnected plates of various thicknesses. For smaller Fe concentrations α-iron nucleation was observed for rolled samples,[19] whereas for well-homogenized samples of $Au_{0.85}Fe_{0.15}$ no traces of α-iron were found.[9,10]

The aim of this work is to clarify the conditions for the nucleation of α-iron, especially in the concentration range below $x = 0.25$, where the ASRO-dependent magnetic properties are found. Using the combination of Mössbauer spectroscopy, wide-angle x-ray diffraction, and small-angle scattering, samples of $Au_{0.85}Fe_{0.15}$ and $Au_{0.75}Fe_{0.25}$ are studied to determine the miscibility gap in the region of small iron concentrations, as well as to get more information on the mechanism of decomposition of Au-Fe within this miscibility gap.

II. EXPERIMENT

Specimens of $Au_{0.85}Fe_{0.15}$ were prepared by electron-beam melting under ultrahigh vacuum ($< 10^{-6}$ Pa) using Au with 99.9999% and Fe with 99.9% purity (enriched to 95% ^{57}Fe). This alloy was used as starting material for the production of $Au_{0.75}Fe_{0.25}$ by addition of natural iron. After the electron-beam melting, the samples of $Au_{0.85}Fe_{0.15}$ and $Au_{0.75}Fe_{0.25}$ were cold rolled to a thickness of 3 and 6 μm, respectively.

Direct-current heating was used for the thermal treatments of each sample by fixing it onto a molybdenum foil connecting two water-cooled copper electrodes in a vacuum better than 5×10^{-5} Pa. The setup allowed reasonably short cooling times (less than 1 min from 900 to 150 °C) within high vacuum. The annealing temperatures

were stable within ± 3 °C. The absolute temperature was controlled to ± 10 °C.

The Mössbauer-spectroscopy measurements were performed at room temperature using a 20 mCi ^{57}Co in Rh standard source with a full width at half maximum of 0.12 mm/s.

Wide-angle x-ray-diffraction measurements were performed with a conventional two-circle diffractometer operated with Cu $K\alpha$ radiation from a 12-kW rotating-anode x-ray generator.

For the small-angle x-ray scattering (SAXS) measurements we used a point-focus camera and Cu $K\alpha$ radiation provided by the same 12-kW x-ray generator. The data were collected using a linear position-sensitive detector. Scattering vectors $k=(4\pi/\lambda)\sin(\theta/2)$ ($\lambda=1.542$ Å: wavelength of the incident x-ray beam, θ: scattering angle) from 0.02 to 0.15 Å^{-1} were accessible. Data were corrected for absorption (determined by measuring the reduction of the scattering from a glassy carbon standard after placing the sample into the primary beam) as well as for electronic background and parasitic scattering from the pinholes. Some of the samples were also measured at the synchrotron beamline JUSIFA in Hamburg with $\lambda=1.78$ Å, which corresponds to a wavelength of the incident x-ray beam just above the absorption edge of iron. Comparison of these measurements with those using Cu $K\alpha$ radiation allowed the estimation of the background due to Fe fluorescence. This background appeared to be small but, nevertheless, all SAXS data collected with Cu $K\alpha$ radiation were corrected for Fe fluorescence.

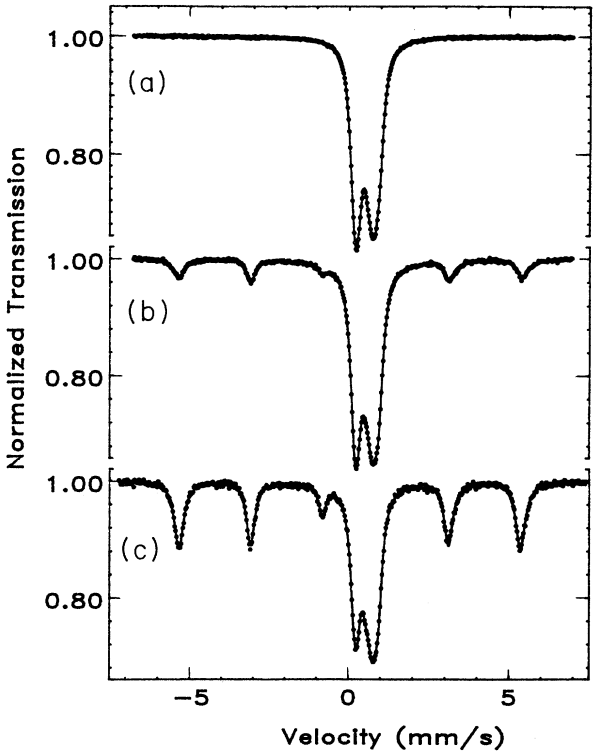

FIG. 1. Mössbauer spectra measured for (a) an as-rolled sample of $Au_{0.75}Fe_{0.25}$ and after an anneal of the rolled sample at 250 °C for (b) 1 day and (c) 10 days.

III. RESULTS

A. Mössbauer spectroscopy

Mössbauer spectra were recorded after the various thermal treatments summarized in Table I. As an example the time evolution of the Mössbauer spectrum of $Au_{0.75}Fe_{0.25}$ annealed at 250 °C after rolling is shown in Fig. 1. The spectra for the as-rolled samples of $Au_{0.75}Fe_{0.25}$ [Fig. 1(a)] and $Au_{0.85}Fe_{0.15}$ show the presence of iron within the Au-Fe solid solution. It has already been demonstrated in earlier studies[9,10] that such spectra can be analyzed using a superposition of several lines

TABLE I. Summary of the results obtained by Mössbauer spectroscopy (F_α^M, with an uncertainty of ≈ 0.02) and by x-ray diffraction (F_α^D, with an uncertainty of ≈ 0.05) for the fraction of iron atoms present as α-Fe. x_e is the concentration of iron atoms inside Au-Fe solid solution in equilibrium with α-Fe (Sec. III B).

Average Fe Composition x (at. %)	Thermal treatment Initial state	Temperature (°C)	Time (d)	F_α^M Eq. (2) (%)	F_α^D Eq. (5) (%)	ρ Eq. (6)	Equilibrium Fe Composition x_e (at. %)
25	Rolled			0	0	0	
		250	1	15	13	0.23	12
		250	10	39	34	1.14	12
		340	2	36	30	1.50	15
	Recrystallized			0			
		340	2	2			
		420	1	2			
15	Rolled			0			
		250	3	8			
		250	6	12			
	Recrystallized			0			
		250	3	0			
		250	6	0			

originating from different nearest-neighbor environments of the Fe-probe atoms.

These as-rolled samples were then subjected to various thermal treatments inside and outside the miscibility gap.[15]

(1) During anneals below 200 °C no change at all was observed in the Mössbauer spectra, even after one week, whereas above this temperature the line shapes changed significantly.[9,10,19] The temperature range around 200 °C therefore corresponds to the freezing in of Fe mobility in the Au-Fe alloy.

(2) A treatment at high temperatures (outside the miscibility gap) changes the line shapes, but Fe remains in solid solution. An analysis of the lines in terms of different environments of the Mössbauer probe atoms was carried out in a previous study.[10] Therein changes in the line shapes from the as-rolled to the annealed state were attributed to short-range ordering of the alloy.

(3) According to the phase diagram[14,15] of Au-Fe, below ≈ 500 °C for $Au_{0.75}Fe_{0.25}$ and ≈ 300 °C for $Au_{0.85}Fe_{0.15}$, α-Fe should coexist with the solid solution.

When a *cold-rolled* sample is annealed in the intermediate temperature range inside the miscibility gap (i.e., between 200 and 500 °C for $Au_{0.75}Fe_{0.25}$ or between 200 and 300 °C for $Au_{0.85}Fe_{0.15}$), after only one day there is the appearance of a six-line spectrum, corresponding to ferromagnetic α-iron precipitates in addition to the Mössbauer line from the solid solution [see Fig. 1(b)]. Such results were also obtained by Whittle, Cywinski, and Clark,[19] for samples of $Au_{80}Fe_{20}$, treated in a similar way. If, however, a sample of $Au_{0.85}Fe_{0.15}$ is *first homogenized* for several days at 900 °C, there is no formation of α-Fe even after an anneal of one week in the temperature range between 200 and 300 °C.[10] The nucleation of α-iron in $Au_{0.85}Fe_{0.15}$ can, therefore, be completely suppressed by a long-term high-temperature treatment. A strong, although not complete, suppression of α-Fe nucleation by a high-temperature treatment is also found for $Au_{0.75}Fe_{0.25}$ (see Table I). This suggests that the limiting factor for α-Fe nucleation is the dislocation density. Reducing the amount of dislocations and grain boundaries by recrystallizing treatments leads to suppression of the precipitation.

In order to get a quantitative evaluation of the amount of α-Fe formed in samples with high dislocation densities, we use the fact that the fractions of iron atoms present in ferromagnetic α-Fe (F_α^M) and in the paramagnetic Au-Fe solid solution (F_p^M) are given by

$$F_\alpha^M = \lambda A_\alpha / f_\alpha^{\mathrm{DW}} ,$$
$$F_p^M = \lambda A_p / f_p^{\mathrm{DW}} , \tag{1}$$

where A_α and A_p are the areas below the Mössbauer lines corresponding to α-Fe and the paramagnetic phase, respectively, and f_α^{DW} and f_p^{DW} are the corresponding Debye-Waller factors. λ is a normalization constant, defined in such a way that $F_\alpha^M + F_p^M = 1$, and therefore,

$$F_\alpha^M = \frac{A_\alpha f_p^{\mathrm{DW}}}{A_\alpha f_p^{\mathrm{DW}} + A_p f_\alpha^{\mathrm{DW}}} . \tag{2}$$

To get an estimate for Debye-Waller factors f^{DW}, we use the Debye model in the form[20]

$$f^{\mathrm{DW}} = \exp\left\{ -\frac{3E^2}{mc^2 k_B \Theta} \left[\frac{1}{4} + \left(\frac{T}{\Theta} \right)^2 \int_0^{\Theta/T} \frac{y\,dy}{e^y - 1} \right] \right\} , \tag{3}$$

where E is the resonant absorption energy (14.4 keV), m the mass of the absorber nucleus (^{57}Fe), c the velocity of light, k_B the Boltzmann constant, T the temperature (≈ 293 K), and Θ the Debye temperature. For α-Fe we take $\Theta = 470$ K,[21] which yields $f_\alpha^{\mathrm{DW}} = 0.83$ at room temperature, in good agreement with the work of Kovats and Walker.[20] The Debye temperature for Fe in the Au-Fe solid solution may be estimated from the temperature dependence of the Mössbauer resonance fraction. Using the data published in Ref. [10] (Fig. 5 therein), we find $\Theta \approx 280$ K for $Au_{0.85}Fe_{0.15}$ at room temperature, yielding $f_p^{\mathrm{DW}} \approx 0.59$. Extrapolating the concentration dependence of the Debye-Waller factor [Fig. 5(a) in Ref. 10], we estimate $\theta \approx 300$ K for $Au_{0.75}Fe_{0.25}$ at room temperature, which means $f_p^{\mathrm{DW}} \approx 0.63$. Using these values and Eq. (2), the fractions F_α^M of iron atoms present in the samples as α-Fe were determined. The results are given in Table I.

B. X-ray diffraction

X-ray diffraction patterns were recorded for samples in the rolled state and after various thermal treatments. Typical line shapes for the (331) and (420) Bragg reflexions from the as-rolled sample of $Au_{0.75}Fe_{0.25}$ are shown in Fig. 2(a). From the initial information gathered by diffractometer measurements, it is possible to obtain the average iron content of the Au-Fe alloys from the composition dependence of the Au-Fe lattice parameter.[14] The iron concentrations determined by this method agree up to $\pm 1\%$ with the nominal compositions. The peaks for $Au_{0.75}Fe_{0.25}$ [Fig. 2(a)] are very broad (about 1.5° full width at half maximum) due to the enormous amount of distortions introduced by the rolling procedure. Indeed, after a recyrstallization treatment above 700 °C the peak width is reduced to $\approx 0.4°$, which corresponds to the resolution of the diffractometer setup. Further thermal treatments of recrystallized samples did not further change the shape of the diffractometer patterns significantly.

In agreement with the Mössbauer measurements, a drastic change in the line shapes occurs when an as-rolled sample of $Au_{0.75}Fe_{0.25}$ is annealed between 200 and 500 °C without a preceding recyrstallization treatment. This is shown in Figs. 2(b) and 2(c) where the development of a second family of Bragg peaks can be seen, resulting finally in a splitting of all reflexions [Fig. 2(c)]. Like the original solid solution, the new family of Bragg reflexions also corresponds to a face-centered-cubic structure but with a larger lattice parameter, indicating a smaller iron content. This depletion of iron within a part of the fcc matrix occurs simultaneously with the formation of α-Fe as detected by Mössbauer-effect measurements (Fig. 1 and Table I).

The most striking result, however, is the fact that the Bragg peaks are not shifting continuously when the matrix is depleted of iron but rather split into two families. After ten days at 250 °C [Fig. 2(c)] there are still large regions of the sample with the original composition coexisting with regions of much lower iron content. This means that the formation of α iron cannot be a process occurring homogeneously in the sample. Whereas in some regions the nucleation barrier is obviously too high for the formation of α-Fe, it must be considerably lowered in other regions, probably due to the presence of defects. A discontinuous change of the lattice constant has also been observed for concentrated Au-Fe alloys (with iron content between 30 and 50 at. %) annealed inside the miscibility gap.[16] Electron microscopy pictures showed in these cases the discontinuous precipitation of α-Fe at dislocations or grain boundaries forming a lamellar structure or families of interconnected plates of various sizes, known as Widmannstätten patterns.[16–18]

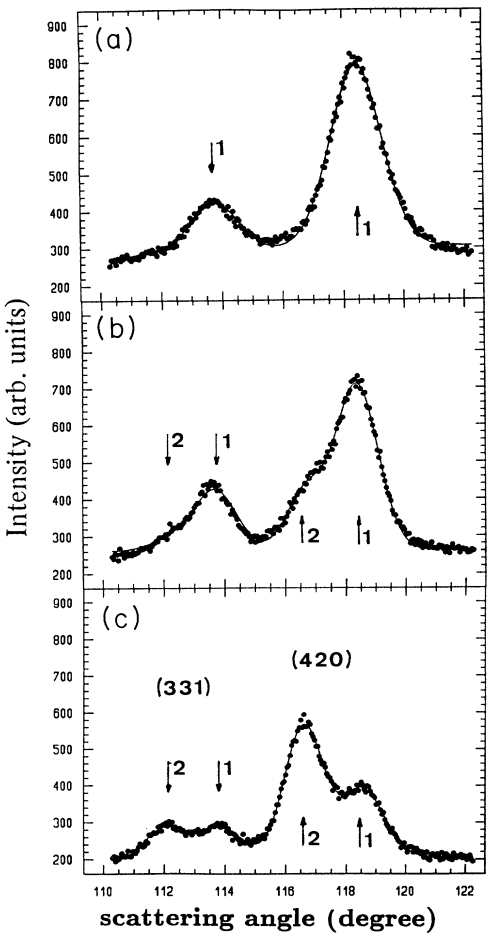

FIG. 2. Wide-angle x-ray spectra for (a) an as-rolled sample of $Au_{0.7}Fe_{0.25}$ and after an anneal of the rolled sample at 250 °C for (b) 1 day and (c) 10 days, in the region of the (331) and (420) Bragg peaks. The arrows indicate the position of the Bragg peaks for a fcc lattice with a lattice constant of 4.008 Å (No. 1) and of 4.047 Å (No. 2). The full line corresponds to a finite of the data with the assumption of a Gaussian line shape for the Bragg peaks (see text).

In order to get a more quantitative evaluation of the iron content in the two sample regions, we have fitted the diffraction patterns assuming constant background and two families of Bragg peaks with Gaussian line shapes, corresponding to two fcc phases with different lattice parameters. The full lines in Fig. 2 show the best fit (using a standard least-squares procedure) under these assumptions. For $Au_{0.75}Fe_{0.25}$ annealed at 250 °C, the two resulting lattice parameters are independent of annealing time and equal to 4.008 and 4.047 Å, corresponding to 25±1 and 12±1 at. % iron in gold, respectively. The enormous change between Figs. 2(b) and 2(c) is only due to changes in the relative amounts of the two fcc phases, their compositions being fixed in time. One of the phases is the original solid solution, where no α-Fe was formed due to the lack of nucleation centers. As the composition of the other fcc phase is also constant in time, we assume that the iron concentration in this phase, x_e, corresponds to the solid solution in equilibrium with α-Fe. The values for x_e are given in Table I for 250 and 340 °C.

In spite of the significant amount of α-Fe, as detected by means of Mössbauer spectroscopy (Fig. 1) in the same samples, no Bragg reflections from the α-iron precipitates could be resolved in the present diffractometer measurements, probably because the iron precipitates were too small to give well-defined Bragg peaks. Nevertheless, the amount of α-Fe may be estimated indirectly from the number of Fe atoms that left the fcc phase. Indeed, calling N the total number of atoms in the sample, and N_x, N_e, and N_α the number of atoms in the two fcc phases (with Fe concentrations x and x_e, respectively) and outside the fcc phases, one can write the conservation laws for iron and gold atoms, respectively,

$$\begin{aligned} &x_e N_e + x N_x + N_\alpha = xN \ , \\ &(1-x_e)N_e + (1-x)n_x = (1-x)N \ , \end{aligned} \tag{4}$$

which give for the fraction F_α^D (D stands for diffraction measurement) of all Fe atoms that left the Au-Fe solid solution

$$F_\alpha^D \equiv \frac{N_\alpha}{xN} = \frac{\rho(x-x_e)}{x[\rho(1-x_e)+1-x]} \ . \tag{5}$$

The ratio $\rho = N_e/N_x$ may, finally, be estimated from the areas B_e and B_x below the equivalent Bragg peaks from the two fcc phases

$$\rho \approx \frac{B_e}{[x_e Z_{\mathrm{Fe}} + (1-x_e)Z_{\mathrm{Au}}]^2} \Big/ \frac{B_x}{[xZ_{\mathrm{Fe}} + (1-x)Z_{\mathrm{Au}}]^2} \ , \tag{6}$$

where Z designates the electron number.

Where the amount of iron depletion was large enough to give a measurable effect in the Bragg peaks, ρ and F_α^D were determined and reported in Table I. It appears that the value of the fraction F_α^D (determined by x-ray diffraction) of iron atoms that left the fcc solid solution is, within the experimental errors, equal to the fraction F_α^M

(determined by Mössbauer spectroscopy) of iron atoms present in the sample as α-Fe. This indicates that no other Fe-rich phase, besides α-Fe, has formed in this sample.

C. Small-angle x-ray scattering

Small-angle x-ray scattering (SAXS) patterns were obtained for all Au-Fe samples, both $Au_{0.75}Fe_{0.25}$ and $Au_{0.85}Fe_{0.15}$. The scattering for the as-rolled samples is (after correction of fluorescence) not completely flat below $k \approx 0.05$ Å^{-1} [stars in Figs. 3(a) and 3(b)], as would be expected for a perfectly homogeneous sample. The SAXS curve remains unchanged, however, by a recyrstallization and homogenization treatment at high temperature. This indicates that the small SAXS signal for the as-rolled sample is mainly due to contributions from the macroscopic surface rather than from precipitates.

A large SAXS signal is, on the other hand, found to develop [open symbols in Figs. 3(a) and 3(b)], if an *as-rolled sample* is annealed in a temperature interval between 200 and 300 °C for $Au_{0.85}Fe_{0.15}$ or between 200 and 500 °C for $Au_{0.75}Fe_{0.25}$. These temperature intervals correspond exactly to those where the discontinuous precipitation of α-iron was found by Mössbauer spectroscopy (Sec. III A) and wide-angle diffraction (Sec. III B). For $Au_{0.85}Fe_{0.15}$, this increase of SAXS during annealing between 200 and 300 °C is totally suppressed in a *recrystallized sample* [Fig. 3(a), full squares]. For $Au_{0.75}Fe_{0.25}$, the increase is strongly reduced [Fig. 3(b), full circles]. This again reflects the fact that the nucleation of α-Fe is connected to the presence of high dislocation density (see Secs. III A and III B).

Additional information on the morphology of the α-iron precipitates may be obtained from the *shape* of the SAXS curves. In Fig. 3 these curves (open symbols) are almost straight lines in a double-logarithmic scale, with a slope close to 3.5. This is extremely different from the scattering functions usually observed from homogeneously distributed precipitates, such as Guinier-Preston (GP) zones.[22] Such scattering functions usually exhibit a maximum due to interference effects between the precipitates or, if the distance between precipitates is too large to give rise to interference effects, the SAXS curve has a Gaussian shape at small values of k.[23] A linear region should then appear in the small-k region of the Guinier plot (logarithm of intensity versus scattering vector squared), with the slope s being related to the radius of gyration R_g of the scattering objects by $s = R_g^2/3$. The Guinier plot of the SAXS data from a sample of $Au_{0.75}Fe_{0.25}$ rolled and then annealed for 2 days at 340 °C is shown in Fig. 4. These data are almost identical with the results published recently for a similar alloy and thermal treatment,[8] where the SAXS intensity was interpreted as evidence for the presence of GP zones. In the present study, however, we find the appearance of this SAXS signal to be due to a massive heterogeneous nucleation of α-iron (see Table I). Moreover, the shape of the SAXS curve itself does not favor an interpretation in terms of small GP zones. Indeed, the slope of the Guinier plot (Fig. 4) is steadily increasing towards small k. For the smallest k accessible to our experiment, the slope (full line in Fig. 4) corresponds to a radius of gyration of ≈ 220 Å. If the SAXS signal was due to isolated precipitates, their radius of gyration would have to be larger than this value, i.e., much too large to account for the strain contrasts observed in electron microscopic studies.[8]

On the other hand, it is known from detailed studies of concentrated Au-Fe alloys[16–18] (with Fe compositions between 30 and 50 at. %) that α-iron nucleates at grain boundaries or dislocations with a lamellar or with a Widmanstätten structure. This last structure consists of interconnected plates of different sizes and has a self-similar character, in the sense that similar morphologies can be seen in the microscope when the magnification is changed. It is well known[24] that self-similar structures give rise to straight SAXS curves, when they are represented on double-logarithmic scales. This is exactly

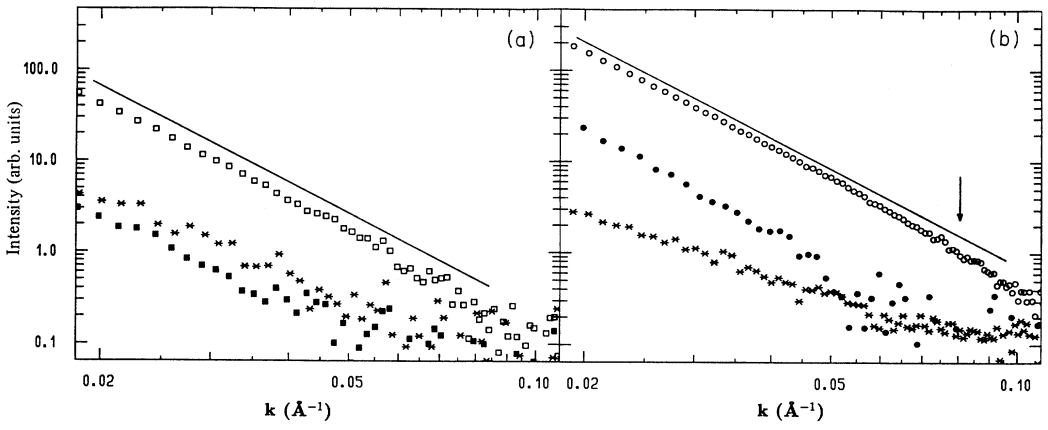

FIG. 3. SAXS patterns for (a) $Au_{0.85}Fe_{0.15}$ and (b) $Au_{0.75}Fe_{0.25}$, where * means the as-rolled samples, □ and ■ annealed for 6 days at 250 °C, and ○ and ● samples annealed for 2 days at 340 °C. The annealing was performed with rolled samples (open symbols) or after a recyrstallization treatment (full symbols). The lines are drawn to show a slope of 3.5, and the arrow indicates the k value, where the slope is changing over to 4.

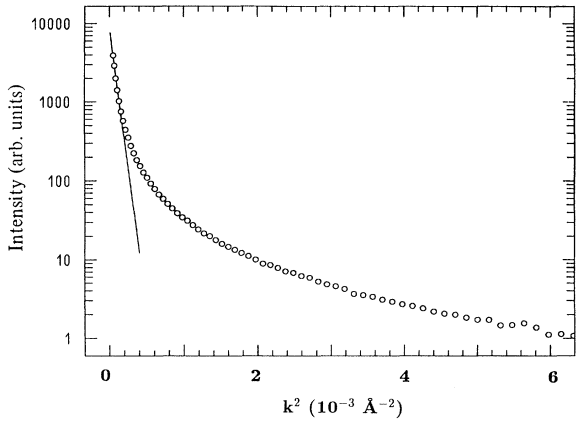

FIG. 4. Guinier plot of the SAXS intensity I vs the square of the scattering vector k for a rolled sample of $Au_{0.75}Fe_{0.25}$ annealed for two days at 340 °C. The full line shows the tangent to the curve in the region of the smallest k accessible to experiment. An interpretation of this slope as $R_g^2/3$ (see text) yields $R_g \approx 220$ Å.

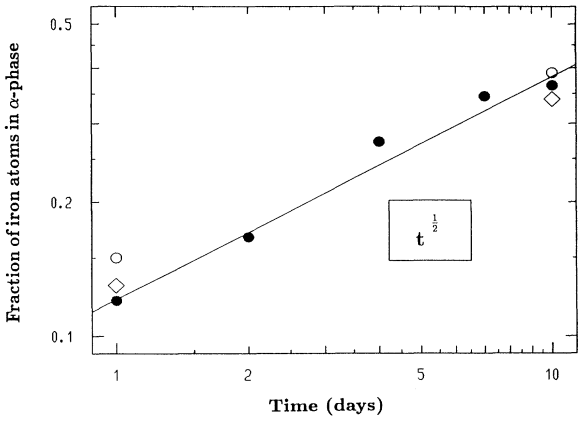

FIG. 6. Time-dependence of the fraction F_α of iron atoms precipitated as α-Fe from ●: the SAXS measurements (normalized so that for $t_0 = 10$ days, $F_\alpha = 0.365$), ○: the Mössbauer measurements, and, ◇: the wide-angle diffraction measurements, plotted in double-logarithmic scales. The full line shows a slope of 1/2.

what we find for the α-Fe precipitates in Au-Fe (Fig. 3). Within the k range of the measurement, the slope is close to 3.5, which would indicate that the self-similar structure corresponds to a surface fractal with a dimension 2.5.[24] Of course, this has to be taken with some caution because the data do not extend over much more than a factor 5 in k. Moreover, for $k > 0.08$ Å^{-1} [arrow in Fig. 3(b)], the curve starts to be steeper with a slope close to 4, in agreement with Porod's law.[25] This indicates that the fractal self-similarity of the surface breaks down at distances smaller than $2\pi/k \approx 80$ Å and behaves then like for an ordinary surface, perhaps because the elementary unit of the "fractal" Fe precipitates structure has a size of about this value.

Furthermore, some information about the *kinetics of the nucleation process* may be obtained from Fig. 5, where

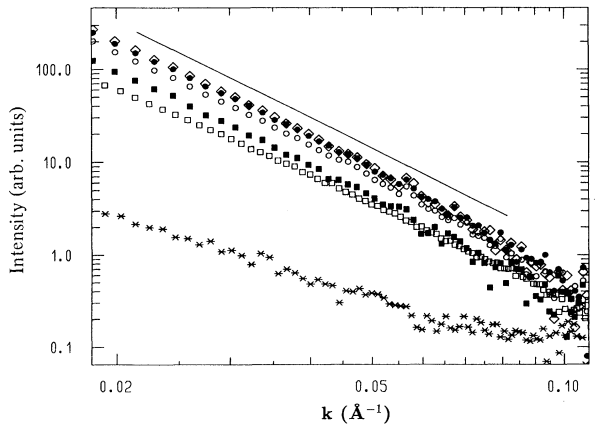

FIG. 5. Temporal evolution of the SAXS intensity $I(k)$ during the anneal at 250 °C of a rolled sample of $Au_{0.85}Fe_{0.15}$. * means the as-rolled state and the annealing time (in days) is □: 1, ■: 2, ○: 4, ●: 7, and ◇: 10. The full line shows a slope of 3.5.

the temporal evolution of the SAXS patterns from a rolled sample of $Au_{0.75}Fe_{0.25}$ annealed at 250 °C is shown. The slope of the SAXS curve in the double-logarithmic scale is 3.5 and does not change very much during time, whereas the total intensity is increasing. As the integral intensity below the SAXS curve is proportional to the total amount of scatterers in the precipitates (that is the amount of Fe present as α-Fe), the increase in SAXS intensity reflects the increase in the amount of α-Fe. Therefore, the relative increase of the α-Fe fraction F_α^S may be estimated directly from the vertical shift of the double-logarithmic representation of the SAXS intensity (Fig. 5). Unlike the case of Mössbauer spectroscopy and wide-angle diffraction, where an absolute value of this fraction was determined, the SAXS results had to be normalized. This was done using the results of Mössbauer measurements and Bragg scattering at $t_0 = 10$ days by setting

$$F_\alpha^S(t_0) = [F_\alpha^M(t_0) + F_\alpha^D(t_0)]/2 = 0.365 \ .$$

The value of $F_\alpha^S(t)$ was then determined at all t and plotted for $Au_{0.75}Fe_{0.25}$ annealed after rolling at 250 °C in Fig. 6, together with the values $F_\alpha^M(t)$ and $F_\alpha^D(t)$ from the other experimental methods. An excellent agreement is obtained for the α-Fe fraction at 1 day. This is an indication for the fact that the SAXS signal from this sample is, indeed, almost entirely due to α-Fe precipitates. Although a systematic study of the growth kinetics was beyond the aim of this work, it may be noted finally that in the particular case of $Au_{0.75}Fe_{0.25}$ annealed at 250 °C after rolling (Fig. 6), the increase of the fraction F_α is consistent with a dependence of the form $F_\alpha(t) \propto \sqrt{t}$.

IV. DISCUSSION AND CONCLUSION

The results of the investigation of α-Fe nucleation in $Au_{0.85}Fe_{0.15}$ and $Au_{0.75}Fe_{0.25}$ by Mössbauer spectroscopy,

x-ray diffraction, and small-angle scattering may be summarized as follows.

(1) Below 200 °C there is no mobility of iron atoms.

(2) For $Au_{0.75}Fe_{0.25}$ there is nucleation of α-iron when an as-rolled sample is annealed between 200 and 500 °C. This nucleation is strongly (although not completely) suppressed by a recrystallization treatment (above $\approx$700 °C) preceding the anneal. For annealing temperatures above 500 °C there is no nucleation of α-iron, even for as-rolled samples, indicating that the solid solution is stable.

(3) For $Au_{0.85}Fe_{0.15}$ there is nucleation of α-iron when an as-rolled sample is annealed between 200 and 300 °C. This nucleation is entirely suppressed by a recyrstallization treatment of the rolled sample. Above 300 °C the solid solution is stable.

(4) When α-Fe nucleates, a splitting of the fcc Bragg reflections occurs, which indicates that there are two different solid solution phases coexisting in the sample with α-Fe. One is the original solid solution and the other a fcc phase with a lower content of iron, which depends only on temperature and not on annealing time. This is interpreted as the composition of a Au-Fe solid solution in equilibrium with α-Fe. This fact can be used to determine the boundary of the miscibility gap, which is shown in Fig. 7. A Bragg-peak splitting has been reported for Au-Fe alloys with higher iron content and interpreted in a similar way.[16] Comparing the present results with those from[16] it appears that the composition of the Au-Fe solid solution in equilibrium with α-iron, obtained from the Bragg peak splitting, is the same for a given temperature regardless of the initial composition of the alloy. The data from[16] are included in Fig. 7 together with those from this work. In addition, points in the phase diagram, where α-iron nucleation was found by Mössbauer-spectroscopy measurements, are marked by full symbols, whereas open symbols show cases where the solid solutions remained stable even for samples with a high dislocation density. We get a perfect agreement between the results by Mössbauer spectroscopy and the miscibility gap determined by x-ray diffraction.

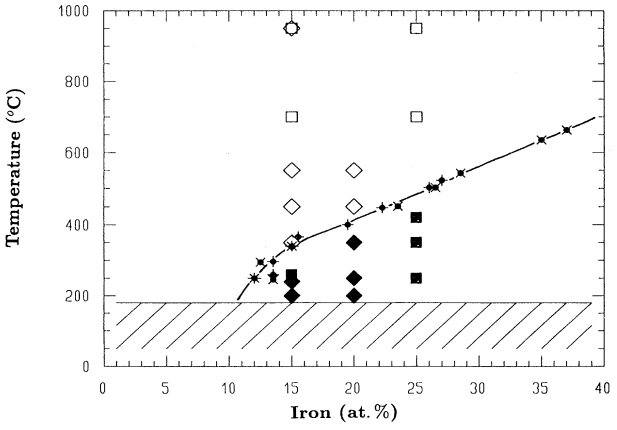

FIG. 7. The miscibility gap of the Au-Fe system is drawn by a full line connecting the values determined by an analysis of the Bragg-peak shifts (see Sec. III B) due to the precipitation of α-iron in ✖: $Au_{0.6}Fe_{0.4}$,[16] ✦: $Au_{0.7}Fe_{0.3}$,[16] and ✷: $Au_{0.75}Fe_{0.25}$ (this work). The full symbols show the conditions under which α-iron nucleation was found in rolled samples, and open symbols where the solid solution was stable, even for samples with high dislocation density (◇: Ref. 9, □: this work). Shaded area: no iron mobility.

(5) A time-dependent SAXS signal is found for samples treated inside the miscibility gap and with a dislocation density large enough to allow the discontinuous precipitation of α-iron. The increase of SAXS intensity occurs simultaneously with the appearance of lines corresponding to ferromagnetic α-iron in the Mössbauer spectra. No evidence is found in the present study for a homogeneous precipitation reaction, such as the formation of GP zones.

(6) The SAXS curve due to the α-iron precipitates nucleated at dislocations or grain boundaries are almost straight lines in a double-logarithmic representation. This may be related to the self-similar character of the Widmanstätten structure, which is the usual morphology for α-iron precipitates in Au-Fe alloy.[16,17] The slope of the SAXS curves would be consistent with a precipitate morphology corresponding to a surface fractal with a dimension around 2.5.

These results indicate that, within the miscibility gap shown in Fig. 7 the solid solution is metastable against the nucleation of α-Fe, but also that the nucleation barrier can be considerably lowered by the presence of dislocations. In cold-rolled $Au_{0.85}Fe_{0.15}$ α-iron nucleates at 250 °C whereas for a recrystallized sample the nucleation barrier is so high that no α-Fe appears even after one week at this temperature (see Table I). It is well known, that heavy rolling induces an inhomogeneous distribution of dislocations, consisting of almost dislocation free cells separated by walls with high dislocation density.[26] Therefore, it is not surprising that the solid solution does not behave like a homogeneous phase with respect to α-Fe nucleation; nucleation starts within the dislocation rich walls or within grain boundaries and depletes the surrounding fcc phase from iron, whereas no precipitation occurs inside the cells, where the density of dislocations is much lower. Reducing the amount of dislocations and grain boundaries by a recyrstallization treatment leads to a (partial) suppression of the precipitation. This suppression is increasingly difficult for alloys with higher Fe content, probably because the boundary of the miscibility gap shifts to higher temperature.

Outside the miscibility gap, results of Mössbauer studies indicate short-range ordering rather than clustering.[9,10] This tendency towards short-range ordering might be the reason why the solid solution is metastable even inside the miscibility gap. Indeed, for a short-range ordered solution the activation energy for the precipitation of iron would be larger than for a random solid solution. This might explain why the precipitation of α-iron does not occur by a homogeneous nucleation process, but needs the presence of dislocations or grain boundaries.

This study does not give evidence for the formation of homogeneously distributed Fe clusters, such as GP zones,

even inside the miscibility gap. The occurrence of small-angle scattering presented as an evidence for GP zones[8] (in a sample of $Au_{0.75}Fe_{0.25}$ annealed for 50 h at 339 °C)[8] is found here to be a consequence of the discontinuous precipitation of α-iron at dislocations and grain boundaries (see Table I). Moreover, and most surprisingly, strain contrasts in electron microscopic pictures, attributed to GP zones oriented along (420) planes,[8,12,13] appear for thermal treatments outside the miscibility gap (such as $Au_{0.82}Fe_{0.18}$ annealed at 500 °C) as well as inside the miscibility gap (e.g., $Au_{0.65}Fe_{0.35}$ aged at 200 °C). This suggest that the strain contrasts are not due to precipitation but to iron-rich (420) planes appearing within the ASRO of the solid solution.

Indeed, iron-rich (420) planes are predicted within the $(1\frac{1}{2}0)$ special-point short-range ordering,[11] and they should induce large distortions due to the difference in size between Au and Fe atoms. The appearance of these planes would only have to follow a kind of "average" periodicity along $\langle 1\frac{1}{2}0 \rangle$ directions in the form of concentration waves,[11] which need not necessarily be visible in electron microscopic images. Furthermore, for Fe plates oriented along (420) with a thickness not exceeding one atomic layer, one would expect a negative first ASRO parameter, since there are no nearest-neighbor sites within one (420) plane. Therefore, the electron microscopic observation of strain constraints due to iron-rich platelets on (420) planes[8,12] and the derivation of a negative first ASRO parameter by Mössbauer spectroscopic measurements[9,10] are both consistent with a $(1\frac{1}{2}0)$ special-point short-range ordering on the Au-Fe solid solution.[27]

Clearly, still more work is needed to elucidate the possible atomic arrangements of iron atoms in Au-Fe. But the present study has shown that for an understanding of the magnetic properties of these alloys, not only the thermal treatment, but also the dislocation density has to be taken into account, since the discontinuous precipitation of ferromagnetic α-iron within the miscibility gap (shown in Fig. 7) is controlled by the presence of such defects.

ACKNOWLEDGMENTS

This work was supported in part by the "Fonds zur Förderng der wissenschaftlichen Forschung." The authors thank G. Vogl for continuous support and are grateful to him and to W. Pfeiler for comments on the manuscript, to P. Szimkowiak for help with sample preparation, and to H. G. Haubold for his support during the measurements at JUSIFA in Hamburg.

*Present address: Hahn-Meitner Institut, Glienicker Strasse 100, D-1000 Berlin 39, Germany.

[1]B. R. Coles, B. V. B. Sarkissian, and R. H. Taylor, Philos. Mag. B **37**, 489 (1978); P. A. Beck, Phys. Rev. B **32**, 7255 (1985); C. Meyer and F. Hartmannn-Boutron, Hyperfine Interact **59**, 219 (1990).

[2]R. J. Borg, D. Y. F. Lai, and C. E. Violet, Phys. Rev. B **5**, 1035 (1972); S. Crane and H. Claus, Solid State Commun. **35**, 461 (1980).

[3]A. F.J. Morgownik and J. A. Mydosh, Solid State Commun. **47**, 325 (1983).

[4]C. E. Violet and R. J. Borg, Phys. Rev. Lett. **51**, 1073 (1983); P. Monod and I. A. Campbell, *ibid.* **52**, 2096 (1984); R. A. Brand and W. Keune, *ibid.* **52**, 2097 (1984); C. E. Violet and R. J. Borg, *ibid.* **52**, 2098 (1984).

[5]E. Dartyge, H. Bouchiat, and P. Monod, Phys. Rev. B **25**, 6995 (1982).

[6]J. W. Cable, G. Parette and Y. Tsunoda, Phys. Rev. B **36**, 8467 (1987).

[7]C. Marsh, S. Polat, and Hadyn Chen, Ser. Metall. **21**, 619 (1987).

[8]Haydn Chen, J. Anderson, K. Ohshima, H. Okajima, and J. Harada, Phys. Rev. B **42**, 2342 (1990).

[9]G. L. White and S. J. Campbell, J. Phys. F **15**, 693 (1985).

[10]Y. Yoshida, F. Langmayr, P. Fratzl, and G. Vogl, Phys. Rev. B **39**, 6394 (1989).

[11]D. de Fontaine, in *Solid State Physics* 34, edited by H. Ehrenreich, F. Seitz, and D. Turnbull, (Academic, New York, 1979), Vol. 34, p. 73.

[12]C. P. Ju, C. M. Wayman, and Haydn Chen, Scr. Metall. **21**, 59 (1987).

[13]Chen-Chia Chou, Haydn Chen, and C. M. Wayman, Mater. Sci. Eng. A **123**, 21 (1990).

[14]E. Raub and P. Walter, Z. Metallkde. **41**, 234 (1950).

[15]O. Kubaschewsky, *Iron-Binary Phase diagrams* (Springer, Berlin, 1982); *Binary Alloy Phase Diagrams,* edited by T. B. Massalsky (American Society for Metals, Ohio, 1986).

[16]M. Frebel and B. Predel, Z. Metallkde. **64**, 913 (1973).

[17]M. Frebel and B. Predel, Mater. Sci. Eng. **15**, 221 (1974).

[18]M. Frebel and J. Schenk, Z. Metallkde. **70**, 55 (1979).

[19]G. L. Whittle, R. Cywinski, and P. E. Clark, J. Phys. F **10** L311 (1980).

[20]T. A. Kovats and J. C. Walker, Phys. Rev. **181**, 610 (1969).

[21]C. Kittel, *Introduction to Solid State Physics* (Oldenburg, Müchen, 1983).

[22]G. Kostorz, J. Appl. Crystallogr. (to be published); J. D. Gunton, M. San Miguel, and Paramdeep S. Sahni, in *Phase Transitions and Critical Phenomena,* edited by C. Domb and J. L. Lebowitz (Academic, New York, 1983), Vol. 8, p. 267.

[23]A. Guinier and G. Fournet, *Small-Angle Scattering of X-Rays,* translated by C. B. Walker (Wiley, New York, 1955).

[24]P. W. Schmidt, in *The Fractal Approach to Heterogeneous Chemistry,* edited by D. Avnir (Wiley, New York, 1989), p. 67.

[25]G. Porod, in *Small-Angle X-Ray Scattering,* edited by O. Glatter and O. Kratky (Academic, London, 1982), p. 17.

[26]R. W. Cahn, in *Physical Metallurgy,* edited by R. W. Cahn and P. Haasen (North-Holland, Amsterdam, 1983), Chap. 25, p. 1595.

[27]D. de Fontaine, Acta Metall. **23**, 553 (1980).